Environment International 128 (2019) 37–45

Contents lists available at ScienceDirect

Environment International

journal homepage: www.elsevier.com/locate/envint

Facile synthesis of electrospun carbon nanofiber/graphene oxide composite aerogels for high efficiency oils absorption

Ying-Zheng Lin[a,c], Lu-Bin Zhong[a], Shuai Dou[a,c], Zai-Dong Shao[a], Qing Liu[a], Yu-Ming Zheng[a,b,c,*]

[a] CAS Key Laboratory of Urban Pollutant Conversion, Institute of Urban Environment, Chinese Academy of Sciences, 1799 Jimei Road, Xiamen 361021, China
[b] CAS Center for Excellence in Regional Atmospheric Environment, Institute of Urban Environment, Chinese Academy of Sciences, Xiamen, Fujian 361021, China
[c] University of Chinese Academy of Sciences, 19A Yuquan Road, Beijing 100049, China

ARTICLE INFO

Handling Editor: Hefa Cheng

Keywords:
Oil spill treatment
Absorbent
Absorption performance
Open porous structure
Electrospinning
Liquid-assist collector

ABSTRACT

Oil contamination will seriously affect the health of water environment, so it is necessary to design ideal oil absorbents with large absorption capacity and high selectivity for effectively purify the oil contaminated water. Preparing high performance carbon aerogel for oil absorption has attracted growing attention, but challenges remain. Here we report a facile approach to fabricate mechanical strength enhanced three-dimensional (3D) nanofibrous aerogel principally through supporting agent liquid assisted collection-electrospinning technology, in which the immersion work was applied to measure the immersion capacity of nanofibers according to liquid-solid interfaces theory. Particularly, electrospun polyacrylonitrile (PAN) nanofibers (NFs) were collected directly in graphene oxide (GO) aqueous dispersion, and the continuous fibrous skeleton assembled with two-dimensional (2D) GO sheets to form open porous networks during the electrospinning process, which basically avoided the tedious preparation steps (nanofiber membrane cutting and re-crosslinking) that have been used previously. Due to the open porous networks promising structure stability of the aerogel, the GO sheets content required in the aerogel stacking process was largely reduced, and there was no strict requirement on the pre-freezing temperature and manner in the subsequent freeze-drying process. Furthermore, followed by thermal treating the PAN NFs/GO composite aerogel, fluffy carbon nanofibers/GO aerogels (CNF/GOAs) were obtained, which exhibited ultra-low density (2–3 mg/mL) and great compressibility (80%). After hydrophobic modification of polydimethylsiloxane by vapor deposition, the CNF/GOAs performed high absorption capacity (120–286 wt/wt) toward diverse oils. Owing to the fire-resistance and great elasticity, the CNF/GOAs could be recycled simply by combustion or mechanical squeeze, and still showed great absorption capacity after 10 cycles, which were feasible for large scale application.

1. Introduction

With another large oil spill accident in the Indian Ocean occurring in June 2017, of which a tanker containing over 5000 tons of oil on board sank, it once more strengthens the urgent need to develop effective control measures for accidental oil spill (ITOPF, 2018). Oil spill can seriously affect the human population and the environment (Obida et al., 2018). To date, many oil spill remediation technologies have been developed, such as oil boom, oil skimmer, oil absorbent, diffusion, combustion and biodegradation (Ma et al., 2016). Compared to other techniques, physical absorption is considered to be the simplest and most economical method, which could quickly remove oil spill with less environmental impact in emergency treatment (Maleki, 2016). However, commercial oil absorbents such as polypropylene sheets generally showed poor absorption efficiency in terms of capacity and selectivity (Wei et al., 2003).

To fill in these gaps, many researchers have focused on designing ideal oil spill absorbents with large absorption capacity and high selectivity (Ge et al., 2016). Among them, carbon-based aerogels have attracted much attention owing to their ultra-low density and high porosity (Maleki, 2016). The main building blocks of carbon-based aerogels include biochar (Bi et al., 2013; Han et al., 2016; Y.Q. Li et al., 2014), carbon fibers (Liang et al., 2012; Wu et al., 2013), carbon nanotubes (CNTs) (Gui et al., 2010; Gui et al., 2013) and graphene (Bi et al., 2012; J. Li et al., 2014). Biochar carbon aerogels (CAs), although being relatively cheap and ecofriendly, often have low absorption capacity and poor mechanical strength (Han et al., 2016). Compared to biochar CAs, CNTs based aerogels, which have high absorption

* Corresponding author at: CAS Key Laboratory of Urban Pollutant Conversion, Institute of Urban Environment, Chinese Academy of Sciences, 1799 Jimei Road, Xiamen 361021, China.
E-mail address: ymzheng@iue.ac.cn (Y.-M. Zheng).

https://doi.org/10.1016/j.envint.2019.04.019
Received 12 January 2019; Received in revised form 26 March 2019; Accepted 8 April 2019
Available online 25 April 2019

capacity, are receiving increasing attention. For example, highly porous CNT sponges with 99% porosity could automatically remove oil film due to their low density and hydrophobicity (Gui et al., 2010). Moreover, to improve their mechanical strength, graphene, which is a single layer of graphite and has unique two-dimensional (2D) structure, was often incorporated into CNT based aerogels (Hu et al., 2014; Kabiri et al., 2014; Wan et al., 2016; Zhan et al., 2018). The hybrid aerogel could sustain large compressive strain ascribing to the cooperation between one-dimensional (1D) CNTs and 2D graphene sheets, thus the absorption saturated aerogel could be conveniently regenerated by compression. Nevertheless, as a high stacking density was required in assembling three-dimensional (3D) aerogel architectures, large consumption of CNTs and graphene significantly increased the production cost. Therefore, designing CA absorbents with economical material cost, excellent mechanical property and high oil absorption performance remains a great challenge.

Currently, there is an increasing trend in preparing affordable CAs, which combine graphene oxide (GO) sheets with other cheap building blocks (Li et al., 2017; Qian et al., 2014; Wang et al., 2015; Xu et al., 2010b). Among them, 1D nanofibers surface as a strong candidate for building blocks (Luo et al., 2018). Electrospinning, a simple and versatile technique for producing nanofiber, has been widely applied to prepare nanofibrous membrane. But the obtained 2D membrane with high bulk density is not practical for oil spill absorption. Today, much attention has been paid to build fluffy 3D electrospun nanofiber-based aerogels, some of which showed extremely low density and recyclable compressibility (Deuber et al., 2018; Si et al., 2014; Xu et al., 2017). However, the preparation procedures were rather tedious and the preparation conditions were strict (Fig. S1). Therefore, a more facile method for building electrospun nanofiber-based CAs is in strong need.

In this paper, a facile method of liquid assisted collection-electrospinning technology combining with freeze drying and thermal stabilization was developed for the preparation of carbon nanofiber-based aerogels (CNFAs) without mechanical dispersing proceeding and chemical crosslinking. In liquid assisted collection-electrospinning, the collecting device was a liquid collector instead of solid plate or drum. Furthermore, GO, which can significantly improve the mechanical strength of CAs, was dispersed in the collecting liquid where continuous polyacrylonitrile (PAN) electrospun nanofibers were collected. Due to PAN nanofibers assembled with GO sheets to generate open porous networks at the micro-scale during electrospinning process, the preparation conditions of following procedure were less stringent, and the amount of GO required for aerogel building was much lower compared to most of studies reported. The ultralight carbon nanofiber/GO composite aerogels (CNF/GOAs) exhibited great compressibility and enhanced mechanical strength compared to CNFAs in the uniaxial compression test. After hydrophobic modification, CNF/GOAs exhibited great absorption capacities toward a wide variety of oils. Moreover, the saturated CNF/GOAs can be easily regenerated by combustion or mechanical squeezing due to their fire resistance and recyclable compressibility, thus showed promising potential in oil spill and organic solvents leakage cleanup.

2. Materials and methods

2.1. Materials

Potassium permanganate ($KMnO_4$), concentrated sulfuric acid (H_2SO_4, 98%), hydrogen peroxide (H_2O_2, 30%), hydrochloric acid (HCl), ethanol, *N*,*N*-dimethylformamide (DMF), and *N*,*N*-dimethylacetamide (DMAc) were of analytical grade and purchased from Sinopharm Chemical Reagent Co. Ltd. (Shanghai, China). Pristine graphite flakes (325 mesh) were purchased from Qingdao Jinrilai graphite Co. Ltd. (Qingdao, China). Polyacrylonitrile (PAN, M_w = 90,000) and poly(methyl methacrylate) (PMMA, M_w = 120,000) were commercially available from Kunshan Hong Yu Plastic Co. Ltd. (Suzhou, China). All the above chemicals were used as-received without further treatment. Polydimethylsiloxane (PDMS) stamps (Sylgard184, Dow Corning) fabrication process is that the PDMS (pre-polymer) and Sylgard184 (curing agent) mixed in acetone at 10:1 ratio and stirring, then the mixture was poured on glass slides to form a thick layer after acetone volatilized in air.

2.2. Preparation of electrospun nanofiber aerogels (NFA_S)

PAN solution (10 wt%) was prepared by dissolving PAN powder in the mixed solvent of DMF and DMAc at ratio 1:1 (w:w). The resultant solution was continuously stirred in a water bath at 60 °C for 2 h. The spinning solutions (PAN/DMF/DMAc) were transferred to a 20 mL syringe connected with a 19-gauge stainless steel needle. The feeding rate was controlled at 1.5 mL/h by a Veryark TCI-IV syringe pump (Guangxi, China). High positive voltage +10 kV and negative voltage −5 kV was constantly applied between the needle tip and a liquid vessel (water or ethanol). The distance between the needle tip and the surface of collecting vessel was 15 cm. The PAN fibrous dispersion was collected after specific electrospinning time (20 min, 40 min, 80 min, and 120 min) to obtain the specific fibrous density of 1 mg/mL, 2 mg/mL, 4 mg/mL, and 6 mg/mL, respectively. Next, 50 mL of the PAN nanofibrous dispersions were placed in 100 mL beakers to shape them as cylinders and frozen in the refrigerator for 4 h. The frozen dispersions were then freeze-dried in a lyophilizer for 48 h to form NFAs.

2.3. Preparation of hydrophobic CNF/GOAs

GO was prepared by oxidizing natural graphite powder via a modified Hummers method (Chen et al., 2016). For CNF/GOAs preparation, the collection liquid in electrospinning process was changed to GO aqueous dispersions with a series of concentrations (0.25 mg/mL, 0.5 mg/mL, 1 mg/mL, and 2 mg/mL). The electrospinning and freeze-drying procedures were same as above, and the PAN fibrous density was set at 1 mg/mL. Finally, nanofibers/GO composite aerogel (NF/GOAs) were transformed to ultralight CNF/GOAs after thermal treatment including pre-oxidation at 250 °C in air for 1 h and low-temperature carbonization at 600 °C in N_2 for 1 h. For comparison, the CNFAs were also prepared by thermal treating the NFAs. To obtain hydrophobic aerogel, CNF/GOAs and a PDMS stamp were placed in a sealed glass container and heated at 234 °C for 1 h.

2.4. Characterization

The morphologies CNFAs and CNF/GOAs were acquired by a Hitachi S-4800 field emission scanning electron microscopy (FESEM). The element composition analysis of the hydrophobic CNF/GOAs was examined by an energy dispersive X-ray spectrometer (EDAX) (Genesis, XM2). Fourier transform infrared (FTIR) spectra of CNFAs and CNF/GOAs were obtained using a Nicolet iS10 spectrometer with a scan range of 4000–400 cm^{-1}. X-rap photoelectron spectroscopy (XPS) analyses were carried out on a ULVAC PHI 5000 Versaprobe III instrument. The contact angles of all samples were measured with 2 μL droplets of liquid using the contact angle measuring system (Dataphysics OCA15EC) at room temperature. The stress-strain curves of the CNFAs and CNF/GOAs were measured by universal material testing machine (KaiQiangLi KD-II 10/100 N, China) using a 10-N load cell in a controlled strain-rate mode with strain rate of 10%/min.

2.5. Oil absorption of the CNF/GOAs

The hydrophobic CNF/GOAs were immersed in the oils for 30 s until saturation. Then, the samples were taken out and allowed to remove redundant liquid molecules that loosely attached to the outermost surface of the aerogel though cohesive and adhesive forces by filter paper. The weight gain ratio of the CNF/GOAs was defined as Q_e, which

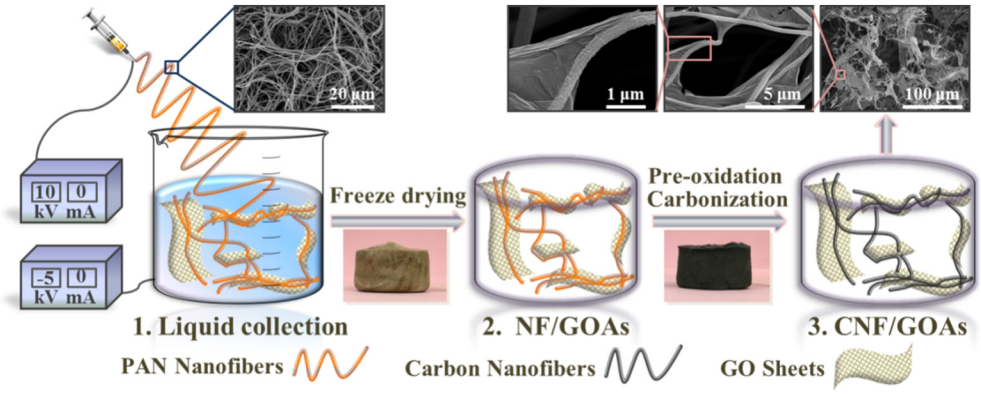

Fig. 1. Schematic diagram shows the main preparation procedure of CNF/GOAs: (1) continuous electrospun PAN nanofibers were collected by GO aqueous dispersion; (2) 3D NF/GOAs were prepared by freeze drying the PAN nanofibers/GO sheets aqueous dispersions; (3) CNF/GOAs were prepared by thermal treatment of NF/GOAs including pre-oxidation and carbonization.

can be calculated according to Eq. (1):

$$Q_e = \frac{m_{saturated} - m_{dry}}{m_{dry}} \quad (1)$$

where m_{dry} and $m_{saturated}$ are the mass of the virgin CNF/GOAs and the aerogel after saturated absorption.

3. Results and discussions

3.1. Fabrication of 3D CNF/GOAs

The principle preparing steps for the CNF/GOAs are shown in Fig. 1. PAN nanofibers assembled with GO sheets to generate open porous networks at the micro-scale during electrospinning process as electrospun PAN nanofibers directly collected in GO aqueous dispersion. By freeze-drying and thermal treatment, the fluffy ultralight 3D CNF/GOAs with open porous networks were obtained. Liquid assisted collection was crucial for 3D architecture building of the aerogels: during electrospinning process, the nonsolvent spontaneously moved into the inter space of fibrous network, and the stereoscopic spaces between nanofibers were increased. Thus, the electrospun nanofibers formed homogeneous continuous nanofibrous skeleton inside collecting liquid. In contrast to liquid collection, 2D electrospun nanofibers membranes that compactly accumulate on solid plane collector showed poor dispersity when immersed in the same nonsolvent (Fig. 2a). By in-depth analysis of the underlying solid-immersing mechanism in electrospinning-liquid collection process, the cooperation between electrospinning solution and collecting liquid played an important role.

According to liquid-solid interfaces theory, the immersion capacity of nanofibers could be measured by immersion work ($-W_i$) that represented as the following equation:

$$-W_i = \sigma_{g-l}\cos\theta \quad (2)$$

where σ_{g-l} is the surface tension of the collecting liquid and θ is the contact angle of nanofibers toward the collecting liquid. When $-W_i > 0$ and $\theta \leq 90^{\circ}$, the nanofiber could be soaked. The immersion work represents the replacing capacity of collecting liquid to the gas near the fibrous solid surface. For example, PAN nanofibers could be immersed homogeneously in both of pure water and 50% ethanol, while PMMA fibers could only be immersed in 50% ethanol (Fig. 2b), because the PMMA fibers exhibited apparent water contact angle > 90° (Fig. S2). In this study, PAN was chosen to be carbon precursor, and GO sheets which served as supporting agents were dispersed homogeneously in pure water to be the collecting liquid, so that PAN fibers could be immersed into the GO aqueous dispersion quickly and then assembled with GO sheets during electrospinning. Upon water removal by sublimation, only the nanofibrous skeleton and GO sheets retained in original states.

As shown in Fig. 2c, compared with the NFAs which were not assembled with GO sheet, the NF/GOAs appeared to be light brown due to homogeneously dispersion of GO sheet in the fibrous skeleton. Previous reported NFAs that prepared by mechanical dispersing 2D membranes relied much on the pre-freezing temperature and manner to induce the micro-length fibers to accumulate around the solvent crystals and form cellular pore structure (Deuber et al., 2017; Deuber et al., 2018; Si et al., 2014; Xu et al., 2017). By contrast, the open porous network of the CNF/GOAs was formed in the initial electrospinning process, thus there were no restrict requirements on pre-freezing process. The final shapes of CNF/GOAs were determined by pre-freezing shapes, thus diverse shapes of CNF/GOAs were obtained by packing the PAN

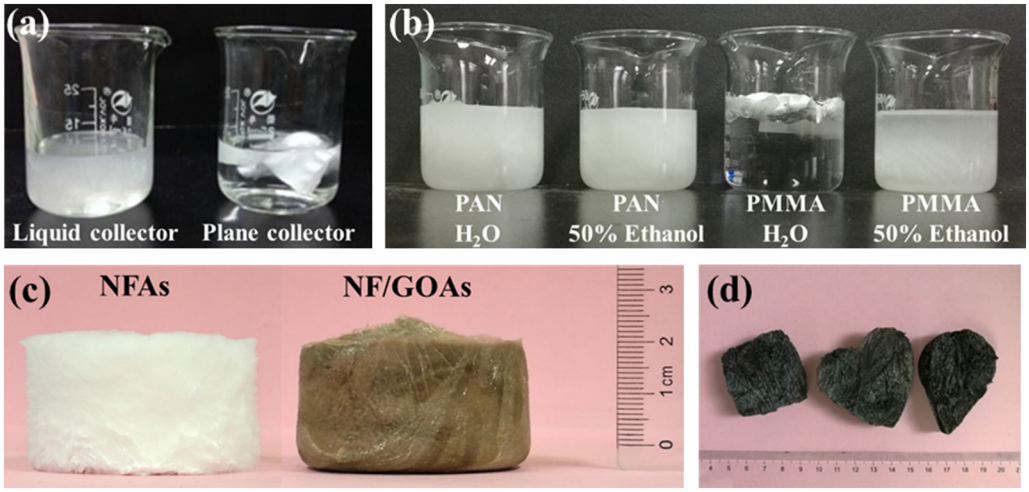

Fig. 2. Analysis of 3D aerogel architecture building requirements and optical photographs of the aerogels in preparation process. (a) Different dispersibility of PAN nanofibers collected by deionized water and 2D PAN nanofibrous membrane in deionized water. (b) PAN and PMMA nanofibers showed different dispersibility in pure water and 50% ethanol. (c) An optical photograph of NFAs and NF/GOAs. (d) An optical photograph of resultant CNF/GOAs in diverse shapes.

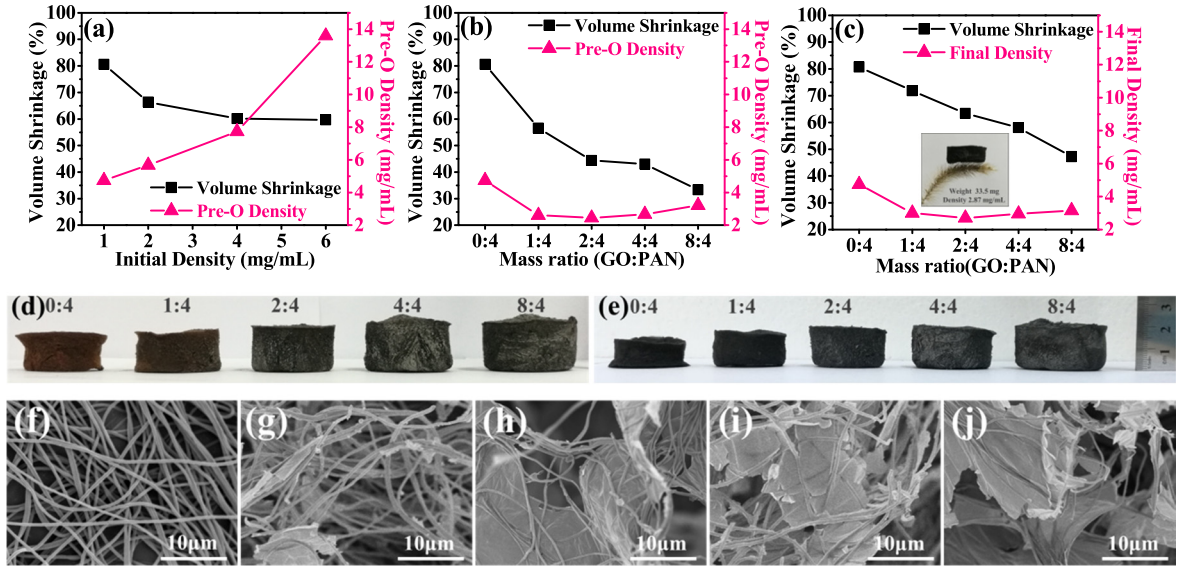

Fig. 3. Exploring proper GO:PAN mass ratios for 3D CNF/GOAs in order to obtain ultralight aerogels with stable structure after thermal treatment. (a) PAN NFAs with different initial densities showed serious volume shrinkage and highly incremental density during pre-oxidation (pre-O) treatment. Volume shrinkage ratio and density of the aerogels with different initial GO:PAN mass ratios (initial density of 1 mg/mL, 1.25 mg/mL, 1.5 mg/mL, 2 mg/mL, and 3 mg/mL) (b) after pre-O treatment and (c) after carbonization. Inset: A CNF/GOA stood on the *Setaria viridis* showing ultralow density (initial mass ratio 2:4, weight 33.5 mg, final density 2.87 mg/mL). Optical photographs of (d) pre-O NF/GOAs and (e) CNF/GOAs with progressive GO:PAN mass ratios (0:4, 1:4, 2:4, 4:4 and 8:4). (f–j) SEM images of CNF/GOAs with progressive GO:PAN mass ratios.

nanofibers/GO aqueous dispersion in different shapes of vessels (Fig. 2d). Meantime, densities of the aerogels could be simply altered by adjusting fibers loading inside the collector, such as extending electrospinning time, increasing spun solution concentration, or changing the volume of collecting solution.

Previous studies (Qian et al., 2015; Rahaman et al., 2007; Zhu et al., 2002) showed that pre-O treatment before carbonization would make the carbon nanofibers made from PAN nanofibers contain more stable chemical structures, since the linear PAN molecular chains converted to aromatic ladder structures, thus the pre-O NFAs turn out to be elastic (Fig. S3). However, due to dramatic chemical structure change, the pre-O NFAs tend to collapse with decreased volume and correspondingly increased densities, thus the mechanical strength of the NFAs in thermal treatment should be further improved (Fig. S3). Density is a key factor in affecting the mechanical property of NFAs, because the continuous fibrous skeletons possess the self-supporting ability. As shown in Fig. 3a, with increasing initial fibrous stacking density the volume shrinkage of pre-O NFAs were reduced. But the mechanical enhancement was limited; the volume shrinkage of the pre-O NFAs was still as high as about 63% when initial density increased to 6 mg/mL, and the resulting pre-O density got much higher, which were not feasible for oil absorption. Therefore, we introduced GO sheets to further improve the mechanical strength and produce ultralight composite aerogel.

The supporting effect of GO sheets was investigated by setting different GO:PAN mass ratios (0:4, 1:4, 2:4, 4:4 and 8:4) in which the PAN density was fixed at 1 mg/mL and then calculating volume shrinkage after thermal treatment. With the assist of GO sheets, the volume shrinkage rate of NF/GOAs in per-O treatment reduced largely compared with NFAs, and the aerogel remained ultra-low density (Fig. 3b and d). For example, with same initial density of 2 mg/mL, the NF/GOAs (GO: PAN mass ratio = 4:4) exhibited volume shrinkage of 43% and density of 2.67 mg/mL under pre-O treatment, which were much lower than those of the NFAs (66%, 5.67 mg/mL). Furthermore, the supporting effects of GO sheets were still obvious after carbonization, and the volume shrinkages were effectively retarded with the increasing of GO ratio (Fig. 3c and e). The resulting CNF/GOAs showed ultralow density ranging from 2 to 3 mg/mL such as the one that could stand steady on the *Setaria viridis* (Fig. 3c inset) with density of about 2.7 mg/mL. The corresponding SEM images of the CNF/GOAs with different GO:PAN ratios showed their different microstructure (Fig. 3f–j). When initial GO:PAN mass ratio increased from 1:4 to 2:4 and 4:4, much more GO sheets were filled into fibrous cross area to form integrated open pore networks. But much more GO sheets were free standing without combining with fibers when the ratio reach to 8:4, which indicated that the GO sheets were overloaded. Therefore, the CNF/GOAs with an initial PAN fibers density of 1 mg/mL and GO:PAN mass ratio of 2:4 were applied in the following mechanical property measurement and absorption test. In addition, based on the continuous fibrous skeleton in CNF/GOAs with self-supporting ability, the GO:PAN mass ratio of 2:4 with relatively less GO addition (0.5 mg/mL) in our aerogels preparation was much smaller than that of 4 mg/mL previous reported (GO:PAN mass ratio = 4:2) where the aerogels were fabricated by micro-length nanofibers and GO sheets (Huang et al., 2016), in other words, the material costs were reduced.

3.2. Mechanical and chemical structure characterization

Uniaxial compression tests were carried out to evaluate the compressibility and compressive strength of CNFAs and CNF/GOAs (Fig. 4a and b). Two distinct stages were observed on the stress-strain curves, an initial linear region at $\varepsilon < 50\%$ and a densification region at $\varepsilon > 50\%$ with tangent module increasing steeply, which indicates their inner open porous structure (Fig. 4c) (Kim et al., 2012). At the first stage, compression made air escape from interspace; owing to their high porosity and flexibility, the stress value was low (< 1 kPa), and the tangent module kept stable. Interestingly, turning points at approx. 20% strain in the initial linear region were observed in Fig. 4b, which were mostly ascribed to the different strength of CNF and GO sheets in the CNF/GOAs. As pressure increased, the CNFs and GO sheets were compacted that induced the curve slope to increase. Meanwhile, compression caused substantial energy dissipation due to friction between flowing air and aerogel skeleton thus generating hysteresis loops in single cycle tests at different strains (20%, 40%, 60%, and 80%). Although with the same initial stacking density, CNF/GOAs showed smaller final densities because of their less volume shrinkage in thermal treatment compared to CNFAs, but the CNF/GOAs exhibited greater

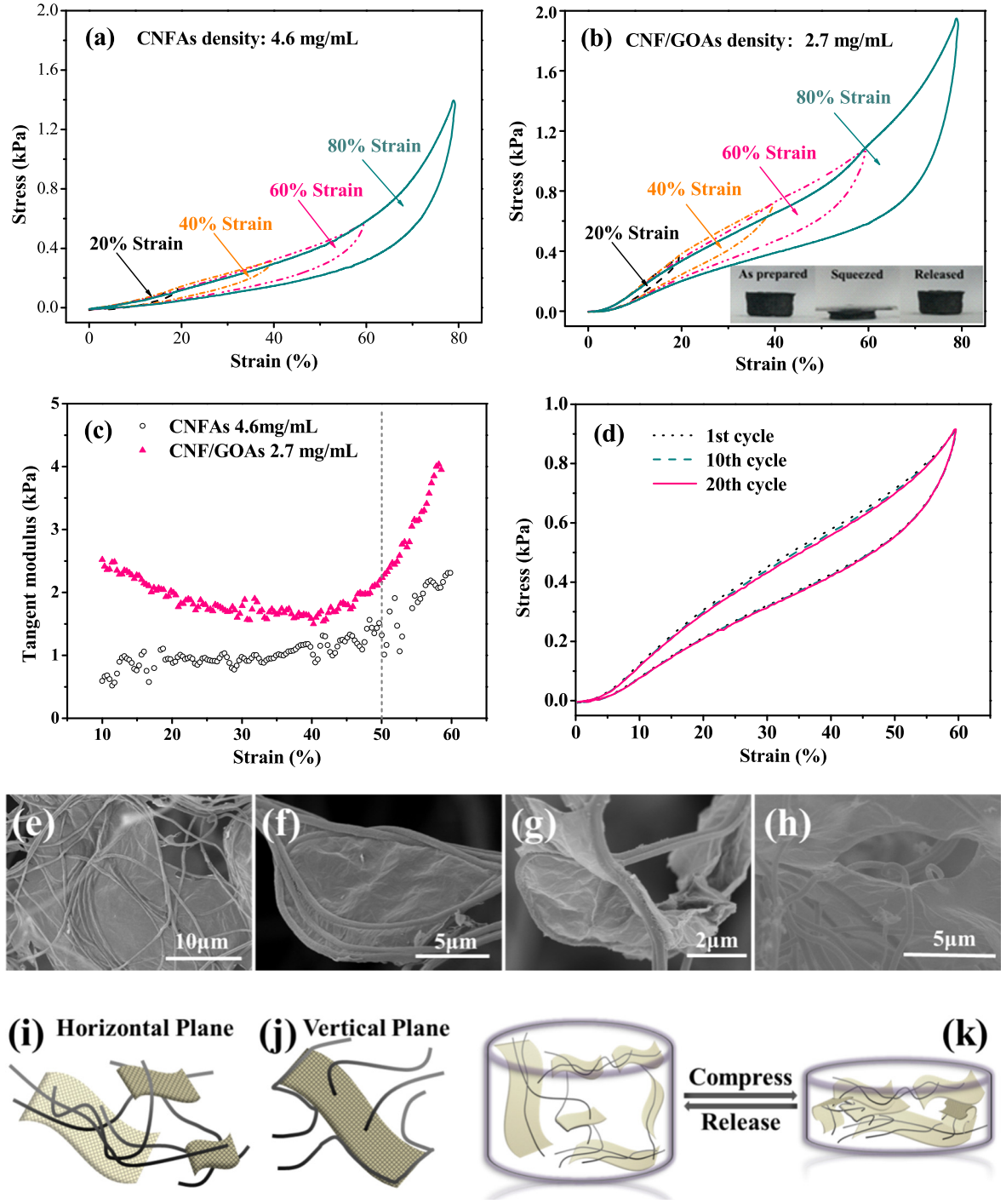

Fig. 4. Compressive mechanical property tests of CNFAs and CNF/GOAs, and microscopic structures of the CNF/GOAs. (a–b) Stress-strain (σ-ε) curves of CNFAs and CNF/GOAs (same initial density 1.5 mg/mL, different final density) on different strains (20%, 40%, 60% and 80%). Inset: photographs of CNF/GOAs under a compressing and releasing cycle. (c) Comparison of tangent modulus change between CNFAs and CNF/GOAs on 60% strain. (d) 20 cyclic compressive test of the CNF/GOAs on 60% strain. (e–h) SEM images of diverse assembling forms between nanofibrous skeleton and GO sheets. (i–j) Cartoon models of 2D GO sheets assembled with 1D CNFs on horizontal and vertical planes. (k) Schematic model of change in an open porous network in the compressing and releasing process.

mechanical strength according to stress-strain curves (Fig. 4a and b). The maximum stress of CNF/GOAs at 80% strain was 1.95 kPa which was larger than the CNFAs (1.41 kPa), and the average tangent modulus in linear region was also enhanced from 0.92 kPa to 1.55 kPa with the assist of GO sheets (Fig. 4c). The result implied that the mechanical strength of CNF/GOAs was improved by GO sheets, which was consistent with the apparent difference of volume shrinkages between CNFAs and CNF/GOAs in thermal treatment described above.

In cyclic compression test, the CNF/GOAs were subjected to 20 loading–unloading fatigue cycles at a large ε of 60% (Fig. 4d). The curve almost maintained initial shape with slight plastic deformation (0.4%), which highlights their structural robustness and promises of practical application. Because the continuous nanofibrous skeletons in CNF/GOAs not only provides self-supporting ability independently but also could be cooperated with GO sheets in diverse formations to form open porous networks, the CNF/GOAs exhibited enhanced compressive strength in compression test and less volume shrinkage in thermal treatment. The SEM images (Fig. 4e–h) presented different combining

formations between the nanofibrous skeleton and GO sheets. On the direction of GO sheets plane, as the supporting layer, a majority of fibers lay down on the large-scale GO sheets by crossing in different space angles; while the middle-scale GO sheets served as a crosslinked bond at the intersection of nanofibers (Fig. 4e, f and i). Apart from horizontal plane, fibers that vertically traversed along GO sheets' edges or penetrated through the GO planes were observed (Fig. 4g, h and j). All these combining formations made up the open porous networks and indicated the elastic mechanism of the CNF/GOAs (Fig. 4k): deformation of the open pore structures in the whole networks rather than nanofibers displacement or GO sheet sliding under external pressure (Sun et al., 2013b). Similarly, although the 3D structure of NFAs tended to collapse due to the dramatic change of chemical structure in single fibers during thermal treatment, these combinations between fibrous skeletons and GO sheets prevented fibers from largely displacement thus reduced the volume shrinkage.

NF/GOAs were gone through thermal treatments including pre-oxidation in air at 250 °C and low-temperature carbonization in nitrogen at 600 °C, both of which affect the chemical structure of PAN nanofibers. After pre-oxidation, the nanofiber color changed from white to brown due to the formation of ladder structure (Fig. S3) (Rahaman et al., 2007). EDX element composition analysis of NF/GOAs showed that carbon content considerably increased while the contents of nitrogen and oxygen reduced after carbonization, which confirmed the element change in thermal treatment (Table S1) (Qian et al., 2015; Zhu et al., 2002). The bonding configurations of nitrogen atoms in CNFAs and CNF/GOAs were characterized by high resolution N 1s XPS spectra (Fig. S4a and b). Both of them could be fitted into four peaks at 398.5, 399.3, 400.2, and 401.4 eV, respectively, corresponding to the pyridine-like, pyrrole-like and graphitic nitrogen, which was associated with cyclization of linear PAN molecular chains during thermal treatment. As introduction of GO sheets, the CNF/GOAs showed increased oxygen content compared with pure CNFAs (Fig. 5a), and the high resolution C 1s XPS spectra indicated that the increased oxygen content were partly attributed to carboxyl groups on GO sheets (Fig. S4c and d). According to the FTIR of CNFAs and CNF/GOAs (Fig. 5b), both of them emerged two peaks at 1579 cm^{-1} and 1292 cm^{-1}, of which the former was ascribed to C═N, C═C and C═O group that also confirmed dehydrogenation and cyclization of the linear PAN molecular chains, and C−C, C−N stretching vibration accounted for the latter. Moreover, due to more carboxyl groups and hydroxyl groups were introduced by the GO sheets, another peak at 3430 cm^{-1} appeared remarkably in the FTIR spectra of the CNF/GOAs which was attributed to the stretching vibration of O−H, and the transmittance at 1579 cm^{-1} was reduced. As reported, the carboxyl groups and hydroxyl groups on GO sheets could form hydrogen bonding with tertiary amino groups in the low-temperature carbonized PAN fibers, which might account for the chemical combination between the carbon nanofibers and the GO sheets (Huang et al., 2016; Sui et al., 2013).

To obtain hydrophobic surface, we treated the CNF/GOAs with PDMS by vapor deposition method that provide a coating over the entire surface of the porous aerogels. The CNF/GOAs and a PDMS stamp were placed together in a sealed glass container; under heat treatment, PDMS degraded to short chains of volatile silicone molecules by partial cleavage of the Si−O bonds, and the low-molecular-weight short PDMS chains formed a conformal layer on the CNF/GOAs surface and subsequently cross-linked (Sun et al., 2013a; Yuan et al., 2008). The wide scan XPS spectrum revealed that the presence of silicon on the inner surface of CNF/GOAs (Fig. 5a), and the newly formed peaks at 102.5 eV and 103.5 eV in the high resolution Si 2p XPS spectrum were corresponded to Si−C and Si−O groups respectively (Fig. S4e). The FTIR of PDMS coated CNF/GOAs also demonstrated a new peak at 671 cm^{-1}, which can be ascribed to the Si−C stretching and CH_3 rocking vibrations (Fig. 5b). Both of the spectra indicated that the short PDMS chains were able to volatilize into the inside of aerogel and re-crosslinked. As anticipated, WCA of CNF/GOAs increased to 146° that was attributed to the low surface energy of PDMS (Fig. 5c). When immersed into water, air bubbles entrapped on the external surface of the CNF/GOAs, which was common property of aerogel materials that applied to oils absorption (Fig. 5d).

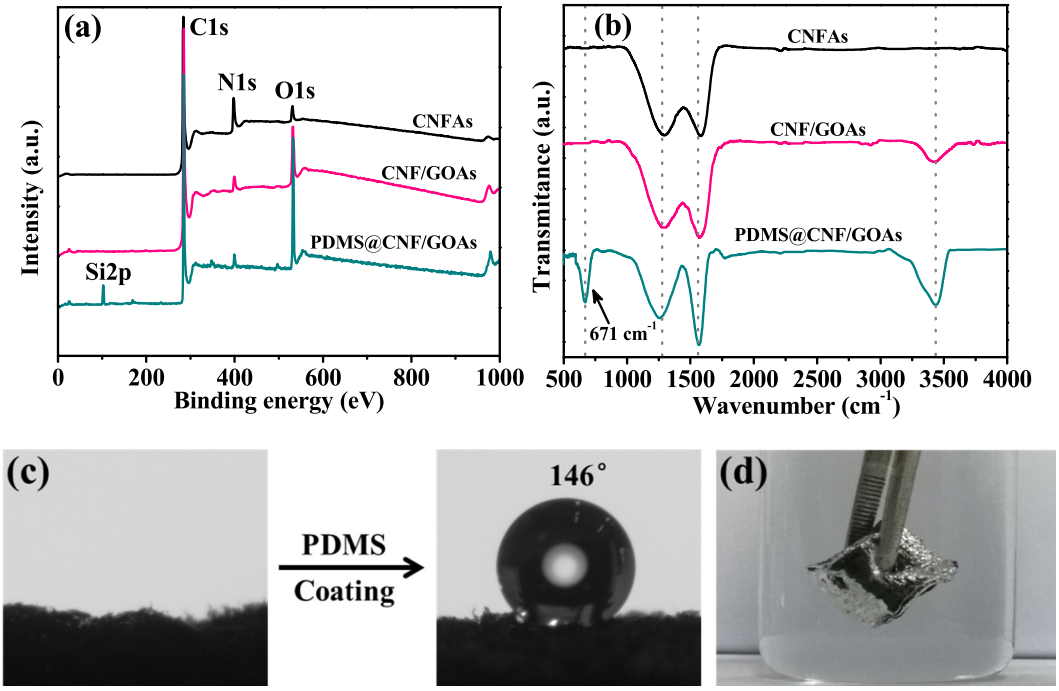

Fig. 5. Chemical structure of CNFAs, CNF/GOAs and hydrophobic modification of CNF/GOAs by PDMS vapor deposition. (a) Wide scan XPS spectra and (b) FTIR spectra of CNFAs, CNF/GOAs and PDMS coated CNF/GOAs. (c) Water contact angle (WCA) measurement of the as-prepared CNF/GOAs (left) and the PDMS coated CNF/GOAs (right). (d) Air bubbles entrapped on the surface of the hydrophobic CNF/GOAs when immersed into water.

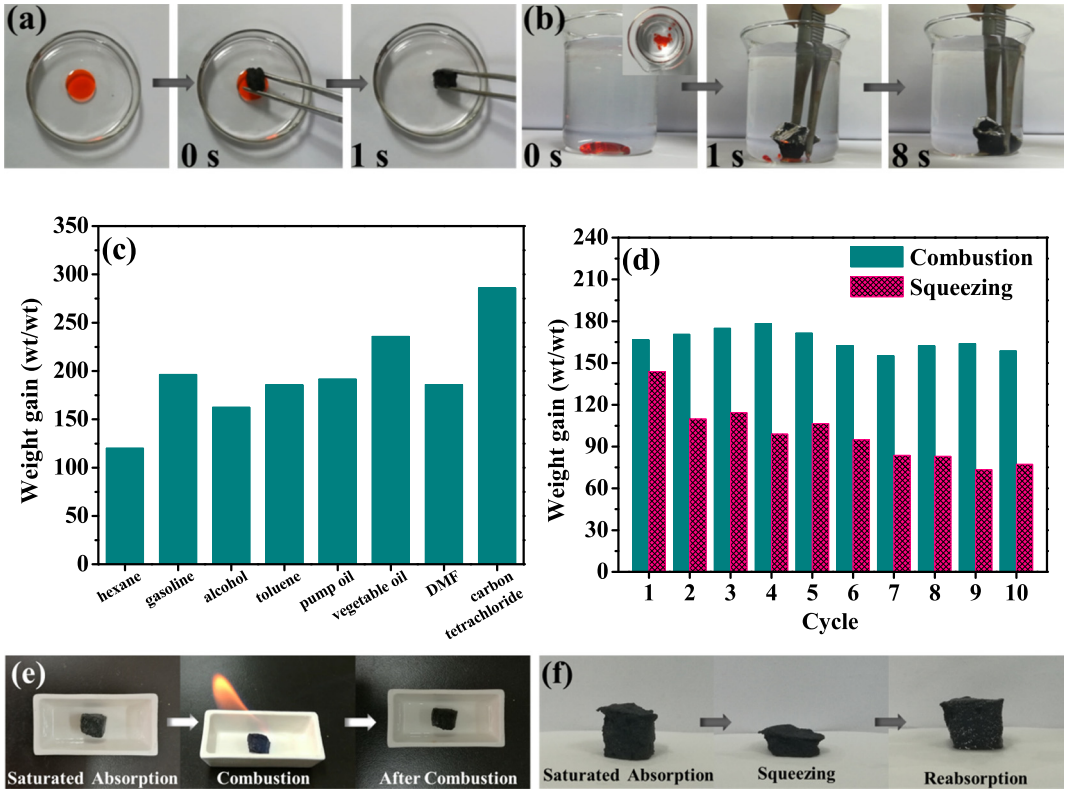

Fig. 6. Oils absorption properties of the hydrophobic CNF/GOAs. The absorption processes of the hydrophobic CNF/GOAs toward (a) toluene on water surface and (b) carbon tetrachloride underwater. (c) Absorption capacity of CNF/GOAs toward diverse oils. (d) Cyclic absorption capacity of CNF/GOAs toward ethanol, which recycled with combustion and squeezing methods, respectively. Regenerate process of CNF/GOAs after saturated absorbing ethanol by (e) combustion and (f) mechanical squeezing.

3.3. Oils absorption performance studies

As expected, the hydrophobic CNF/GOAs that perform overall properties including ultra-low density, strong mechanical property and good hydrophobicity showed excellent selective absorption capacity for the oils from water, in terms of short absorption time, high absorption quantity and good recycling ability. When a piece of hydrophobic CNF/GOAs was put on the surface of toluene-water mixture, toluene (dyed by Sudan red) could be adsorbed into the aerogel in 1 s (Fig. 6a, Movie S1). Carbon tetrachloride (dyed by Sudan red) sank under the water, which represented for high density solvents, could also be fast absorbed by submerging the CNF/GOAs into the polluted areas (Fig. 6b, Movie S2). Notably, there were almost no water uptake being observed during the absorption processes in both of the above experiments, which indicated the excellent hydrophobicity of the aerogel (Fig. S5).

The absorption capacities of CNF/GOAs toward various oils were also investigated. The absorption capacity was measured by weight-gain ratio (Q_{wt}) which is the mass of absorbed solution compared to the mass of virgin CNF/GOAs. As summarized in Fig. 6c and Table 1, the CNF/GOAs showed excellent absorption capacity of 120–286 times to their own weight, which higher than most reported oil absorption aerogels. Noteworthy, it can be also seen that the CNF/GOAs and other graphene/CNT based carbon aerogels represented larger capacity than other aerogel materials, due to their ultra-low densities. However, the graphene-based aerogels required much more raw materials to form stable aerogel structure during the stacking process. Some researches pointed out that the GO sheets density should be at least 2 mg/mL in aerogel stacking process (Lin et al., 2011; Riaz et al., 2017; Xu et al., 2010a), which was four times as much as that of the CNF/GOAs in this work. The largely reduced quantity demand of GO sheets in CNF/GOAs preparation was mainly due to the stably mutual supporting between nanofibrous skeleton and GO sheets, thus the cost of the materials was also cut to a great extent. The different absorption capacities of CNF/GOAs toward diverse adsorbates mainly attributed to their different densities. After normalized the weight gain by the different densities of oils, the CNF/GOAs showed excellent absorption capacity approximated to 200 mL/g (Fig. S6). The deviation from average absorption capacity mainly resulted from the different viscosity of oils. Liquids with higher viscosity showed larger absorbed quantity than the liquid other with similar density, such as gasoline and vegetable oil, because high viscosity liquids would be more likely to attach on the outermost surface of the aerogel by cohesive and adhesive forces.

The reusability of absorbent is one of the most important criteria to evaluate the feasibility of its large-scale application. Owing to the fire-resistant and good mechanical properties, the aerogel could be recycled simply by combustion or squeezing. As shown in Figs. 6d & e and S7, it could be found that the CNF/GOAs almost kept their original shapes after the combustion, and displayed excellent absorption capacity after ten cycles of absorption-combustion with only a little lost in weight gain (5%). The fire resistance mainly attributed to the porous nature of the aerogel that allowed for the quick removal of the heat during combustion (Sun et al., 2013b). Although combustion is an easy way to recycle the aerogel, simple squeezing could be more environmentally friendly to cycle some oils that would cause pollution in combustion. Due to the good mechanical property, it was obvious that the squeezed aerogel could recover to its original shape after re-absorption (Fig. 6f). The CNF/GOAs regenerated by squeezing was also tested for ten cycles, and 53% of the saturated sorption capacity was maintained after ten times of squeezing (Fig. 6d). Part of the residual solvent cannot be squeezed out entirely just by mechanical force leading to the incomplete recovery rate, but the remaining space could still store adsorbed solvent.

A simple economic analysis for the possible mass production of the CNF/GOAs was conducted, and a comparison with existing commercial

Table 1
Absorption capacity comparison of various absorbent materials.

Absorbent materials	Absorbed substances	Absorption capacities (wt/wt)	Ref.
Carbon nanofibers/graphene oxide aerogel	Oils and organic solvents	120–286	Present work
Graphene aerogel	Oils and organic solvents	120–250	(J. Li et al., 2014)
Graphene aerogel	Oils and organic solvents	~40	(Liu et al., 2017)
CNTs sponges	Diesel oil/gas oil	56/49	(Gui et al., 2013)
CNT sponges	Oils and organic solvents	80–180	(Gui et al., 2010)
Carbon aerogels from graphene and CNTs	Oils and organic solvents	215–743	(Sun et al., 2013b)
CNT-graphene hybrid aerogel	Oils and organic solvents	100–150	(Hu et al., 2014)
Carbon fiber aerogel made from raw cotton	Oils and organic solvents	50–192	(Bi et al., 2013)
Carbon aerogel from winter melon	Gasoline/diesel/crude oil	24/27/25	(Y.Q. Li et al., 2014)
Carbonaceous nanofiber aerogels	Oils and organic solvents	40–115	(Liang et al., 2012)
PVA-co-PE nanofibrous aerogels	Oils and organic solvents	25–53.29	(Liu et al., 2018)
Melamine sponge @ZIF-8	Various oils	10–38	(Feng and Yao, 2018)

product (PP sheets) was also disclosed. As shown in Table S2, the raw materials cost for the fabrication of CNF/GOAs was estimated to be approx. 7800 RMB/m^3 or 2890 RMB/kg, which did not include the other costs such as energy and labor. Moreover, the cost for absorbing 1 L of oil by the CNF/GOAs was evaluated and compared with the existing commercial product (PP sheets). As the oil saturated CNF/GOAs could be recycled through combustion or mechanical squeezing for more than ten cycles, the cost of per absorbing one liter oil by the CNF/GOAs could be reduced to around 1.4 RMB, which was much less than the absorption cost (5 RMB) by PP sheets (Table S3). The high absorption capacity, simply recycling procedure and acceptable industrial cost confirm that CNF/GOAs could be applicable and effective as high performance absorbents for oil-spill and organic solvents.

4. Conclusions

In summary, the facile preparation of ultralight carbon aerogels assembled from CNFs and GO sheets named CNF/GOAs demonstrated highly effective for diverse oils absorption. 3D aerogel structures of the CNF/GOAs were feasibly built through collecting electrospun PAN nanofibers in a GO aqueous dispersion, which could obtain a continuous fibrous skeleton and didn't need cross linker. Because the open pore networks constructed by the self-supporting carbon fibrous skeletons and GO sheets prevented the nanofibers and GO sheets from replacement in thermal treatment and compression, the quantity requirement of GO sheets in the aerogel building-up was largely reduced, and the aerogels were highly compressible which is convenient for recycling the absorbed oil by mechanical squeezing. Only 0.5 mg/mL GO sheet assembled with 1 mg/mL PAN nanofibers could build carbon aerogel with stable 3D structure and ultra-low density (2–3 mg/mL), thus the material cost of CNF/GOAs was greatly cut compared to other CNTs/graphene-based aerogels. The CNF/GOAs displayed excellent absorption capacities reaching 120–286 times to its own weight toward diverse oils and organic solvents, which were higher than most reported aerogels. The absorption saturated aerogel could be simply cycled by combustion or mechanical squeezing. The study provides a facile carbon aerogel architecture construction method, and the novel electrospun nanofiber-based aerogel with good absorption and mechanical properties would be beneficial for future application in pollutants absorption.

Supplementary data to this article can be found online at https://doi.org/10.1016/j.envint.2019.04.019.

Acknowledgments

The authors acknowledge the financial support from the National Natural Science Foundation of China (grant nos. 51578525 and 5153000136), and the Fujian Key Laboratory of Advanced Materials (Xiamen University).

References

Bi, H., Xie, X., Yin, K., Zhou, Y., Wan, S., He, L., Xu, F., Banhart, F., Sun, L., Ruoff, R.S., 2012. Spongy graphene as a highly efficient and recyclable sorbent for oils and organic solvents. Adv. Funct. Mater. 22, 4421–4425.
Bi, H., Yin, Z., Cao, X., Xie, X., Tan, C., Huang, X., Chen, B., Chen, F., Yang, Q., Bu, X., Lu, X., Sun, L., Zhang, H., 2013. Carbon fiber aerogel made from raw cotton: a novel, efficient and recyclable sorbent for oils and organic solvents. Adv. Mater. 25, 5916–5921.
Chen, J., Chi, F., Huang, L., Zhang, M., Yao, B., Li, Y., Li, C., Shi, G., 2016. Synthesis of graphene oxide sheets with controlled sizes from sieved graphite flakes. Carbon 110, 34–40.
Deuber, F., Mousavi, S., Federer, L., Adlhart, C., 2017. Amphiphilic nanofiber-based aerogels for selective liquid absorption from electrospun biopolymers. Adv. Mater. Interfaces 4, 1700065.
Deuber, F., Mousavi, S., Federer, L., Hofer, M., Adlhart, C., 2018. Exploration of ultralight nanofiber aerogels as particle filters: capacity and efficiency. ACS Appl. Mater. Interfaces 10, 9069–9076.
Feng, Y., Yao, J., 2018. Design of melamine sponge-based three-dimensional porous materials toward applications. Ind. Eng. Chem. Res. 57, 7322–7330.
Ge, J., Zhao, H.Y., Zhu, H.W., Huang, J., Shi, L.A., Yu, S.H., 2016. Advanced sorbents for oil-spill cleanup: recent advances and future perspectives. Adv. Mater. 28, 10459–10490.
Gui, X., Wei, J., Wang, K., Cao, A., Zhu, H., Jia, Y., Shu, Q., Wu, D., 2010. Carbon nanotube sponges. Adv. Mater. 22, 617–621.
Gui, X., Zeng, Z., Lin, Z., Gan, Q., Xiang, R., Zhu, Y., Cao, A., Tang, Z., 2013. Magnetic and highly recyclable macroporous carbon nanotubes for spilled oil sorption and separation. ACS Appl. Mater. Interfaces 5, 5845–5850.
Han, S., Sun, Q., Zheng, H., Li, J., Jin, C., 2016. Green and facile fabrication of carbon aerogels from cellulose-based waste newspaper for solving organic pollution. Carbohydr. Polym. 136, 95–100.
Hu, H., Zhao, Z., Gogotsi, Y., Qiu, J., 2014. Compressible carbon nanotube–graphene hybrid aerogels with superhydrophobicity and superoleophilicity for oil sorption. Environ. Sci. Technol. Lett. 1, 214–220.
Huang, Y., Lai, F., Zhang, L., Lu, H., Miao, Y.E., Liu, T., 2016. Elastic carbon aerogels reconstructed from electrospun nanofibers and graphene as three-dimensional networked matrix for efficient energy storage/conversion. Sci. Rep. 6, 31541.
ITOPF, 2018. Oil tanker spill statistics. http://www.itopf.org/knowledge-resources/data-statistics/statistics/.
Kabiri, S., Tran, D.N.H., Altalhi, T., Losic, D., 2014. Outstanding adsorption performance of graphene–carbon nanotube aerogels for continuous oil removal. Carbon 80, 523–533.
Kim, K.H., Oh, Y., Islam, M.F., 2012. Graphene coating makes carbon nanotube aerogels superelastic and resistant to fatigue. Nat. Nanotechnol. 7, 562–566.
Li, J., Li, J., Meng, H., Xie, S., Zhang, B., Li, L., Ma, H., Zhang, J., Yu, M., 2014. Ultra-light, compressible and fire-resistant graphene aerogel as a highly efficient and recyclable absorbent for organic liquids. J. Mater. Chem. A 2, 2934.
Li, Y.Q., Samad, Y.A., Polychronopoulou, K., Alhassan, S.M., Liao, K., 2014. Carbon aerogel from winter melon for highly efficient and recyclable oils and organic solvents absorption. ACS Sustain. Chem. Eng. 2, 1492–1497.
Li, C., Wu, Z.Y., Liang, H.W., Chen, J.F., Yu, S.H., 2017. Ultralight multifunctional carbon-based aerogels by combining graphene oxide and bacterial cellulose. Small 13, 1700453.
Liang, H.W., Guan, Q.F., Chen, L.F., Zhu, Z., Zhang, W.J., Yu, S.H., 2012. Macroscopic-scale template synthesis of robust carbonaceous nanofiber hydrogels and aerogels and their applications. Angew. Chem. Int. Ed. 51, 5101–5105.
Lin, Y., Ehlert, G.J., Bukowsky, C., Sodano, H.A., 2011. Superhydrophobic functionalized graphene aerogels. ACS Appl. Mater. Interfaces 3, 2200–2203.
Liu, Y., Shi, Q., Hou, C., Zhang, Q., Li, Y., Wang, H., 2017. Versatile mechanically strong and highly conductive chemically converted graphene aerogels. Carbon 125, 352–359.
Liu, Q., Chen, J., Mei, T., He, X., Zhong, W., Liu, K., Wang, W., Wang, Y., Li, M., Wang, D., 2018. A facile route to the production of polymeric nanofibrous aerogels for environmentally sustainable applications. J. Mater. Chem. A 6, 3692–3704.
Luo, H., Xiong, P., Xie, J., Yang, Z., Huang, Y., Hu, J., Wan, Y., Xu, Y., 2018. Uniformly

dispersed freestanding carbon nanofiber/graphene electrodes made by a scalable biological method for high-performance flexible supercapacitors. Adv. Funct. Mater. 28, 1803075.
Ma, Q., Cheng, H., Fane, A.G., Wang, R., Zhang, H., 2016. Recent development of advanced materials with special wettability for selective oil/water separation. Small 12, 2186–2202.
Maleki, H., 2016. Recent advances in aerogels for environmental remediation applications: a review. Chem. Eng. J. 300, 98–118.
Obida, C.B., Alan Blackburn, G., Duncan Whyatt, J., Semple, K.T., 2018. Quantifying the exposure of humans and the environment to oil pollution in the Niger Delta using advanced geostatistical techniques. Environ. Int. 111, 32–42.
Qian, Y., Ismail, I.M., Stein, A., 2014. Ultralight, high-surface-area, multifunctional graphene-based aerogels from self-assembly of graphene oxide and resol. Carbon 68, 221–231.
Qian, X., Zou, R., OuYang, Q., Wang, X., Zhang, Y., 2015. Surface structural evolvement in the conversion of polyacrylonitrile precursors to carbon fibers. Appl. Surf. Sci. 327, 246–252.
Rahaman, M.S.A., Ismail, A.F., Mustafa, A., 2007. A review of heat treatment on polyacrylonitrile fiber. Polym. Degrad. Stab. 92, 1421–1432.
Riaz, M.A., Hadi, P., Abidi, I.H., Tyagi, A., Ou, X., Luo, Z., 2017. Recyclable 3D graphene aerogel with bimodal pore structure for ultrafast and selective oil sorption from water. RSC Adv. 7, 29722–29731.
Si, Y., Yu, J., Tang, X., Ge, J., Ding, B., 2014. Ultralight nanofibre-assembled cellular aerogels with superelasticity and multifunctionality. Nat. Commun. 5, 5802.
Sui, Z.Y., Cui, Y., Zhu, J.H., Han, B.H., 2013. Preparation of three-dimensional graphene oxide–polyethylenimine porous materials as dye and gas adsorbents. ACS Appl. Mater. Interfaces 5, 9172–9179.
Sun, H., Li, A., Zhu, Z., Liang, W., Zhao, X., La, P., Deng, W., 2013a. Superhydrophobic activated carbon-coated sponges for separation and absorption. ChemSusChem 6, 1057–1062.
Sun, H., Xu, Z., Gao, C., 2013b. Multifunctional, ultra-flyweight, synergistically assembled carbon aerogels. Adv. Mater. 25, 2554–2560.
Wan, W., Zhang, R., Li, W., Liu, H., Lin, Y., Li, L., Zhou, Y., 2016. Graphene–carbon nanotube aerogel as an ultra-light, compressible and recyclable highly efficient absorbent for oil and dyes. Environ. Sci.: Nano 3, 107–113.
Wang, X., Lu, L.L., Yu, Z.L., Xu, X.W., Zheng, Y.R., Yu, S.H., 2015. Scalable template synthesis of resorcinol–formaldehyde/graphene oxide composite aerogels with tunable densities and mechanical properties. Angew. Chem. Int. Ed. 54, 2397–2401.
Wei, Q.F., Mather, R.R., Fotheringham, A.F., Yang, R.D., 2003. Evaluation of nonwoven polypropylene oil sorbents in marine oil-spill recovery. Mar. Pollut. Bull. 46, 780–783.
Wu, Z.Y., Li, C., Liang, H.W., Chen, J.F., Yu, S.H., 2013. Ultralight, flexible, and fire-resistant carbon nanofiber aerogels from bacterial cellulose. Angew. Chem. Int. Ed. 52, 2925–2929.
Xu, Y., Sheng, K., Li, C., Shi, G., 2010a. Self-assembled graphene hydrogel via a one-step hydrothermal process. ACS Nano 4, 4324–4330.
Xu, Y., Wu, Q., Sun, Y., Bai, H., Shi, G., 2010b. Three-dimensional self-assembly of graphene oxide and DNA into multifunctional hydrogels. ACS Nano 4, 7358–7362.
Xu, T., Ding, Y., Wang, Z., Zhao, Y., Wu, W., Fong, H., Zhu, Z., 2017. Three-dimensional and ultralight sponges with tunable conductivity assembled from electrospun nanofibers for a highly sensitive tactile pressure sensor. J. Mater. Chem. C 5, 10288–10294.
Yuan, J., Liu, X., Akbulut, O., Hu, J., Suib, S.L., Kong, J., Stellacci, F., 2008. Superwetting nanowire membranes for selective absorption. Nat. Nanotechnol. 3, 332–336.
Zhan, W., Yu, S., Gao, L., Wang, F., Fu, X., Sui, G., Yang, X., 2018. Bioinspired assembly of carbon nanotube into graphene aerogel with “cabbagelike” hierarchical porous structure for highly efficient organic pollutants cleanup. ACS Appl. Mater. Interfaces 10, 1093–1103.
Zhu, D., Xu, C., Nakura, N., Matsuo, M., 2002. Study of carbon films from PAN VGCF composites by gelation crystallization from solution. Carbon 40, 363–373.